



Fast- and slow-light-enhanced light drag in a moving microcavity

Tian Qin ¹, Jianfan Yang¹, Fangxing Zhang¹, Yao Chen¹, Dongyi Shen², Wei Liu², Lei Chen², Xiaoshun Jiang³, Xianfeng Chen² & Wenjie Wan ^{1✉}

Fizeau's experiment, inspiring Einstein's special theory of relativity, reveals a small dragging effect acting on light inside a moving medium. Dispersion can enhance such light drag according to Lorentz's predication. Here fast- and slow-light-enhanced light drag is demonstrated experimentally in a moving optical microcavity through stimulated Brillouin scattering induced transparency and absorption. The strong dispersion provides an enhancement factor up to $\sim 10^4$, greatly reducing the system size down to the micrometer range. These results may offer a unique platform for a compact, integrated solution to motion sensing and ultrafast signal processing applications.

¹The State Key Laboratory of Advanced Optical Communication Systems and Networks, University of Michigan-Shanghai Jiao Tong University Joint Institute, Shanghai Jiao Tong University, 200240 Shanghai, China. ²MOE Key Laboratory for Laser Plasmas and Collaborative Innovation Center of IFSA, Department of Physics and Astronomy, Shanghai Jiao Tong University, 200240 Shanghai, China. ³National Laboratory of Solid State Microstructures and College of Engineering and Applied Sciences, Nanjing University, 210093 Nanjing, China. ✉email: wenjie.wan@sjtu.edu.cn

It is well-known that the speed of light in a vacuum is the same regardless of the choice of reference frame, according to Einstein's theory of special relativity¹. However, once light propagates in a moving medium, it can be dragged by the host medium, known as Fresnel drag effect², which was first theoretically predicted by Fresnel in 1818 and experimentally verified by Fizeau's experiment in a water-running tube interferometer in 1851³. Later, Lorentz pointed out the influence of dispersion on the light-dragging effect⁴, which was also experimentally verified by Zeeman^{5,6}. All of these works play a very important role in the development of Einstein's special relativity⁷. However, under the circumstance of low or no dispersion, such a light-dragging effect is so insignificant that requires either long traveling path or large velocity of host media for any observable results. Therefore, large light dragging requires strong dispersion to enhance the effect for compact systems and any practical applications such as motional sensing⁸.

Previously, strong dispersion enhanced light drag has been observed in highly dispersive media, such as atomic vapors^{9,10}, cold atoms¹¹, and doped crystals¹², where ultra-narrow linewidth atomic resonances associated strong normal dispersion, e.g. in an electromagnetically induced transparent (EIT) medium¹³, can enormously enhance the drag effect up to $\sim 10^5$ times as compared to low dispersive media like water or glass^{3,5,6}, greatly reducing the system sizes down to the millimeter scale. However, the rigid experimental conditions in these atomic systems, i.e. vacuum and temperature control, highly limit their practical applications. On the other hand, in solid-state systems, photonic crystals^{14,15}, optomechanical devices^{16–20}, and doped crystals^{21,22} have shown great potential for dispersion management in a compact form, allowing exotic propagation such as slow/fast light²³. Particularly, both normal and anomalous dispersion associated with Brillouin scattering-induced transparency/absorption (BSIT/BSIA) have been demonstrated in a micro-scale optomechanical microcavity²⁰, providing a fertile ground to test light drag under both dispersion regimes. Especially, light drag under anomalous dispersion, which has not been experimentally demonstrated yet, is believed to be crucial for improving gyroscopic sensitivity in a high-finesse resonant optical cavity^{8,24}.

In this work, we experimentally demonstrate strong normal and anomalous dispersion enhanced light dragging effect arising from both slow and fast light induced by stimulated Brillouin scattering (SBS) processes in a solid-state microcavity platform. In a high-quality (Q) microcavity, both acoustical and optical waves can be trapped resonantly in whispering gallery modes (WGMs), the high- Q acoustical resonances induce sharp perturbations in optical ones, creating Brillouin scattering-induced transparency or absorption depending on their relative phase. In these spectral disturbed regimes, dispersion relations are strongly altered, resulting in slow or fast group propagation of light. Based on that, Lorentz's predications of light drag are examined with an enhancement factor up to $\sim 10^4$ in both dispersion regimes through a fiber-coupled microcavity in a vibrating mode. Moreover, such optomechanical micro-devices allow actively tuning the induced dispersion. As a result, the light dragging can also be modified accordingly, further validating the nature of dispersion-dependent enhancement. At last, a Fano-like resonance obtained by detuning in the microcavity permits the observation of the drag by both slow and fast light in close spectral proximity. These results extend the special relativity experiment to a new solid-state system at the microscale, opening up new avenues for their practical applications in motional sensing and ultrafast signal processing²⁵ (see Supplementary Note 1).

Results

Theoretical model for enhanced light drag in a BSIT/BSIA microcavity. Our work to investigate the light dragging effect is based on a tapered fiber-coupled microsphere resonator, which vibrates translationally parallel to the coupling fiber to provide the drag (Fig. 1a). Here light can tunnel from the input fiber into the microcavity to form a WGM due to total internal reflection²⁶. Such tunneling occurs in both ways, allowing intracavity light coupled back to the fiber. However, such drag is relatively small, for example, Carmon's team has shown that a millimeter size resonator with $Q_{\text{optical}} \sim 10^6$ spinning at ~ 6000 Hz can only cause ~ 20 MHz nonreciprocal resonance shift for optical isolation²⁵, dispersion can greatly enhance this process and reduce the

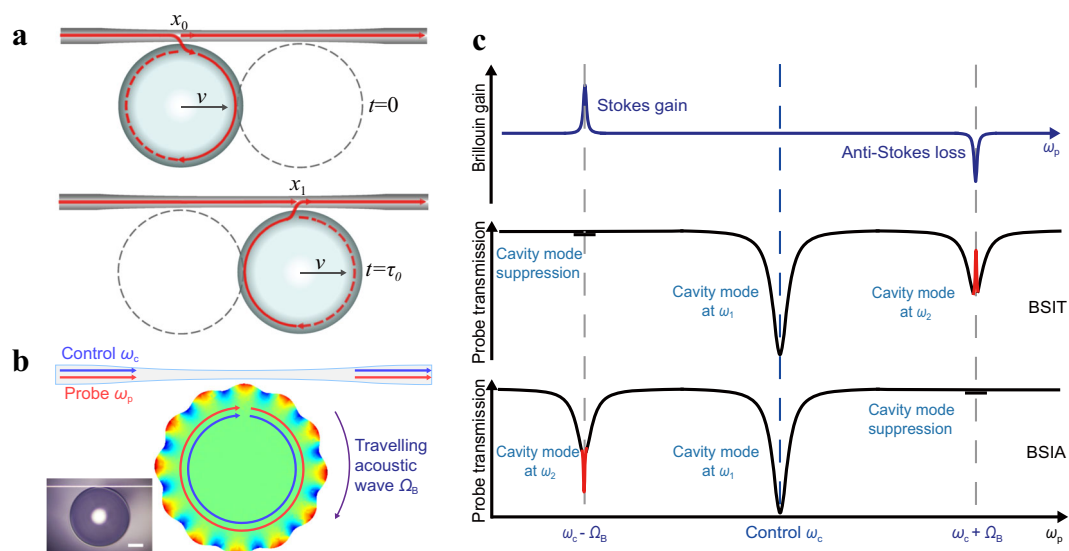


Fig. 1 Light-dragging effect in a BSIT/BSIA microcavity. **a** Illustration of the light-dragging effect in a moving microsphere cavity. **b** Forward Brillouin scattering in a microcavity. The control and the probe lasers in two phase-matched cavity modes are coupled through a forward-traveling acoustic wave. The microscope image of the coupling system is in the inset, with a scale bar of 50 μm . **c** For Brillouin scattering-induced transparency/absorption (BSIT/BSIA), the probe experiences anti-Stokes loss/Stokes gain inside the cavity.

dimension. In the case of BSIT/BSIA^{19,20}, strong dispersion can result in slow/fast light up to microsecond level, similar dispersion can be found in other coupled resonances system^{17,18,27,28}, this opens up a unique window to test light drag.

As shown in Fig. 1b, our microsphere cavity can support both optical and acoustic whispering-gallery-type resonances, where a strong optical pump light is launched into one optical WGM, simultaneously generating a Stokes photon with an extra acoustic phonon, or an anti-Stokes photon via absorbing one phonon through an electrostriction-induced SBS process^{16,19,20}. The Stokes or anti-Stokes processes occur depending on whether an extra optical resonance can be found for the scattering photon as shown in Fig. 1c. This leads to BSIA or BSIT transmission, respectively, due to inherent loss or gain mechanisms²⁹. Meanwhile, it has been reported slow and fast light can reach up to microsecond level²⁰, this can hugely enhance the light drag according to Lorentz's predication⁴.

The mechanism of slow and fast light enhanced light drag in a moving WGM microcavity can be considered by applying Lorentz transformation to the coupling system. Here we assume that light is coupled into a microcavity moving along the tapered fiber at velocity v (Fig. 1a), the round-trip time and the frequency of light with respect to the frame of moving cavity (S') are given by the Lorentz transformation: $\tau'_0 = L n(\omega')/c$, $\omega' = \omega(1 - v/c)$, where L is the perimeter of the cavity, $n(\omega')$ is the refractive index of the cavity in the moving frame. Meanwhile, light is resonantly trapped inside the cavity for a certain period which is further enhanced through the dispersion. By the time the intracavity light is coupled back to the fiber, the cavity has already moved translationally for some distance, effectively dragging the intracavity field towards the direction of motion. Therefore, the moving medium can modify the round-trip phase of internal light accordingly, which is expected to be very small when $v \ll c$. To achieve large dispersion enhancement by means of slow/fast light, a weak probe laser at ω_p is scanned through the Stokes or anti-Stokes resonances induced by a strong control laser at ω_c with SBS as shown in Fig. 1b, c, similar to prior works^{19,20}. This drag can induce phase shift with respect to the remaining light only propagating in the tapered fiber in terms of interference, experimentally this drag phase can be measured by the transmission output through a spectrum scanning combined with a lock-in detection scheme (see Supplementary Note 2).

By considering the dragging effect in term of the refractive index of lasers under the moving frame³⁰ (see Supplementary Note 3), the relative light-dragging phase shift of the probe can be obtained as

$$\begin{aligned} \Delta\phi_{\text{drag-p}}(\omega_p) &\approx \frac{L(r\omega_c - \omega_p)n(\omega_c)v}{c^2} \left[1 + \frac{n_g(\omega_p) - n(\omega_p)}{n(\omega_c)} \right] \\ &\equiv \frac{L(r\omega_c - \omega_p)n(\omega_c)v}{c^2} F_d(\omega_p), \end{aligned} \quad (1)$$

where r is the thermal drift factor³⁰, $F_p(\omega_p)$ is defined as the light-dragging enhancement factor, which is approximately proportional to $n_g(\omega_p)$ with a factor of $1/n(\omega_c)$ when $n_g(\omega_p) \gg n(\omega_p)$. The strong group dispersion $n_g(\omega_p)$ tremendously enhances the dragging effect brought by the velocity v , which is similar to the light drag in the atomic vapors and cold atoms^{10,11}.

In our experiments, the transmission of the probe through the fiber-coupled microcavity system is altered by such light-dragging-induced phase shift through interfering with the residual light inside the fiber³¹, giving us a tool to measure the

dragging phase shift (see Supplementary Note 4)

$$\begin{aligned} \Delta T_{\text{drag-p}}(\omega_p) &\approx \frac{2a\kappa_2(1-a^2)(1-\kappa_2^2)\Delta\phi_0(\omega_c \pm \Omega_B)}{[(1-a\kappa_2)^2 + a\kappa_2\Delta\phi_0^2(\omega_c \pm \Omega_B)]^2} \times \Delta\phi_{\text{drag-p}}(\omega_p) \\ &\equiv C \cdot \Delta\phi_{\text{drag-p}}(\omega_p), \end{aligned} \quad (2)$$

where a is the round-trip absorption loss of the cavity, κ_2 is the coefficient of transmission between the tapered fiber and the cavity, Ω_B is the frequency of the acoustic wave, $\Delta\phi_0(\omega_c \pm \Omega_B)$ is the initial round-trip phase mismatch of the cavity at anti-Stokes/Stokes frequency, depending on the case of slow light(+) or fast light(-). It is convenient to define a parameter C to characterize the effect of small phase perturbation on the transmission near an optical resonance. Then the phase shift induced by dispersion enhanced light-dragging effect can be converted into the change of probe transmission.

Slow-light-enhanced light drag in a BSIT microcavity. Firstly, we realize BSIT through an anti-stokes process in our optomechanical microcavity (see "Methods" section). Figure 2a depicts an ultra-narrow mechanical resonance peak (3 kHz linewidth) inside an optical cavity mode (22.4 MHz linewidth), similar to the previous works^{19,20}. Its phase spectrum in Fig. 2b exhibits a rapid climb near the center of the induced transparency window, which later will be explored for the light-dragging enhancement. Meanwhile, we observe a slow light with time delay up to 338 μs (Fig. 2c) by probing a secondary light through BSIT window, which is related to the group index by (see Supplementary Note 5):

$$n_g(\omega_p) \approx -\frac{\tau_g(\omega_p)\pi c}{L\mathcal{F}}, \quad (3)$$

where τ_g is the probe time delay, $F_d(\omega_p)$ is the finesse of the cavity. Then n_g is calculated to be -3.5×10^4 , which can provide a light dragging enhancement for up to -2.4×10^4 according to Eq. (1). Note that a time delay is associated with a negative n_g in the BSIT due to output coupling from the intracavity field²⁰ (see Supplementary Note 5), which is totally opposite to the case of atomic systems. Based on this platform, we exam dispersion enhanced light drag by vibrating the microcavity along the fiber while keeping a constant coupling gap so that the relative speed is sinusously modulated (see Supplementary Note 6).

Here the microsphere is fabricated on the top of a fiber, effectively composing a cantilever that oscillates at several mechanical resonances³² in Fig. 2d. We choose two of these resonances (at 59 and 62 kHz) driven by an attached piezoelectric vibrator (Fig. 2e) for maximizing moving speed to exam any observable dragging effect. This is done by reading out the transmission of the probe laser whose frequency is periodically (4 Hz) scanned through one slow-light window (in 20 kHz frequency range), meanwhile, the microcavity cantilever's vibration frequency is slowly swept through those two resonances (with a repetition rate of 10 mHz in the range of 2.5 kHz). As a result, small dips in the envelope of probe transmission are observed periodically on slow-varying background humps (Fig. 2e), which arise from the superposition of light-dragging effect (dips) and coupling-gap modulation (humps) as shown in Supplementary Note 7. These dips are measured through a lock-in technique recording the temporal modulation induced by the light drag of the vibrating cantilever. Ideally, the coupling gap is kept constant if perfectly aligned. However, slight misalignment can lead to a huge response in the transmission exhibiting a background hump. The relative motion of the vibrating microcavity is calibrated to give a maximum velocity of 0.12 m/s accompanied with 10 nm

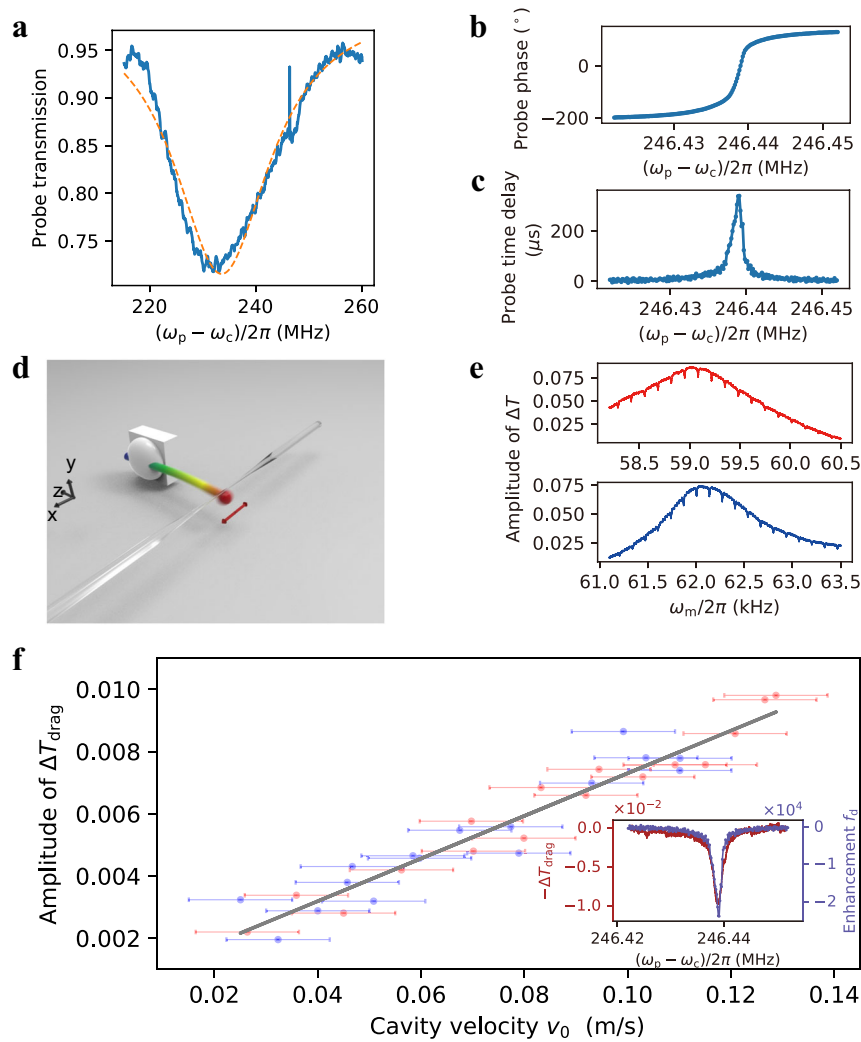


Fig. 2 Light-dragging effect in a BSIT microcavity. **a** Brillouin scattering-induced transparency (BSIT) is observed in an anti-Stokes mode ($Q = 8.6 \times 10^6$). **b** Large positive slope in the probe phase indicates strong normal dispersion. **c** Probe delay of $338 \mu\text{s}$ is observed at the through port, corresponding to an intracavity group index of $n_g = -3.5 \times 10^4$ and $F_d = -2.4 \times 10^4$. **d** Illustration of a vibrating microcavity driven by a piezoelectric vibrator. **e** The amplitude of perturbation on probe transmission near two microcavity vibration resonances. The perturbation is contributed by the light-dragging effect (dips) and coupling-gap modulation (background hump). **f** The light-dragging perturbation, ΔT_{drag} , linearly scales with cavity velocity. The error bars of ΔT_{drag} are smaller than the data points and the x-axis error bars represent the standard deviation of cavity velocity. The inset compares a single dip and corresponding enhancement factor.

change in the coupling gap by monitoring the coupling efficiency with perpendicular alignments of the piezoelectric vibrator.

Such dips in the envelope of transmission are caused by the interference between the direct transmitted light and those dragged by the vibrating microcavity (see Supplementary Note 6). Their height directly measures the dragging phase due to destructive or constructive interferences according to Eq. (1). Under the condition of slow-light enhancement, the amplitude of light-dragging perturbation, measured from the height of the dips linearly scale with the velocity of the microcavity (Fig. 2f), which is calibrated by the displacement and the vibration frequency. This confirms the velocity dependence of light drag in Eq. (2). Meanwhile, since the dragging effect is linearly enhanced by the dispersion, the profile of a dip is compared with the group index near the slow light regime in the inset of Fig. 2f, exhibiting good agreement in height and linewidth.

Fast-light-enhanced light drag in a BSIA microcavity. Anomalous dispersion can also induce strong enhancement to

light drag in a Stokes SBS configuration as shown in Fig. 3. The complex phase of the Stokes-induced acoustical resonance coherently interferes with one optical resonance, resulting in BSIA²⁰ in Fig. 3a, b. Unlike the previous case of BSIT, the phase spectrum of BSIA has a large negative slope at the center of the absorption dip, exhibiting a near-Lorentzian lineshape in Fig. 3c. The central strong dispersion leads to fast light measured by the group time advancement up to $26 \mu\text{s}$ in Fig. 3d. The resulting light drag induces dips in the envelope of perturbation in the transmission. Note that, such dips mix up the coherent interference from both optical resonances, the acoustical resonance as well as light drag (see Supplementary Note 6). The height of the dips can be translated to the light-dragging perturbation, which is characterized to be linearly dependent on the corresponding microcavity velocity (Fig. 3e). Previously, only slow-light media, i.e. normal dispersion, have been implemented for light drag, the current work in a BSIA medium is the first one, to our knowledge, demonstrating anomalous dispersion-enhanced light drag, which is crucial for improving rotational sensing^{8,24}.

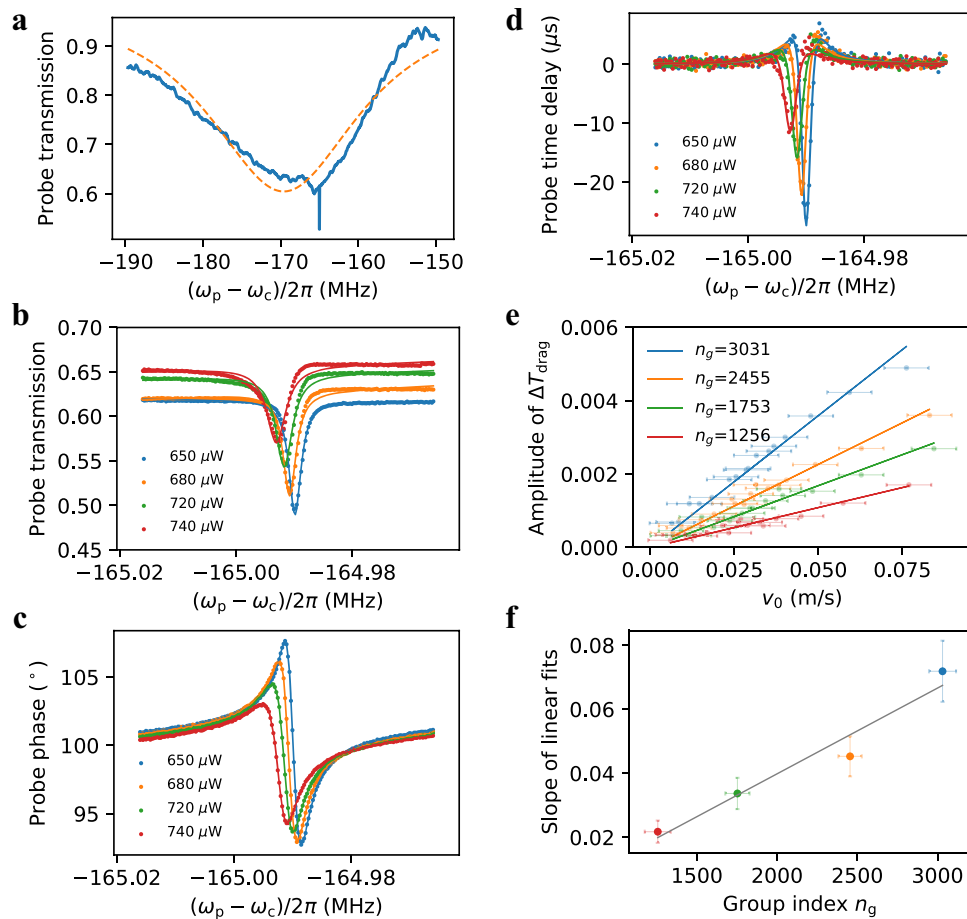


Fig. 3 Light-dragging effect in a BSIA microcavity. **a** Brillouin scattering-induced absorption (BSIA) is observed in a Stokes mode ($Q = 8 \times 10^6$). **b** The linewidth of the absorption window increases with control power. **c** The probe phase exhibits a large negative slope at the center of the absorption window and negative slope on two wings. **d** The probe time advancement reaches $26 \mu\text{s}$ with $650 \mu\text{W}$ control power and the corresponding intracavity group index is calculated to be 3031. The probe time advancement decreases with increasing control power, which implies decreasing intracavity group index of 3031 (blue), 2455 (orange), 1753 (green), and 1256 (red). **e** The light-dragging perturbation, ΔT_{drag} , linearly scales with cavity velocity under different dispersion and the error bars represent the standard deviation. **f** Normalized enhancement factor obtained from the slopes in panel **e** is linearly dependent on group index n_g . The uncertainty on the x-axis comes from the standard deviation of group time delay, while the uncertainty on the y-axis is calculated from panel **e**.

Moreover, we illustrate that such dispersion-enhanced light drag can be actively tunable through dispersion management in Fig. 3. Experimentally, the linewidth of BSIA can be effectively controlled by the pump power through nonlinear Brillouin gain similar to prior work¹⁹ (see Supplementary Note 8). Here the depth of the BSIA transmission dips decreases by around 50% when increasing the pumping power from 650 to 740 μW . More importantly, their linewidths increase (Fig. 3b), resulting in smoother phase jumps (Fig. 3c) and reducing group time advances by half (Fig. 3d). As a result, the corresponding light drag measured under these pumping conditions now exhibits slightly different slopes with respect to the cavity velocity (Fig. 3e), since the enhancement factor F_d has been modified by different dispersion in these configurations. For verification purpose, we plot these slope coefficients from Fig. 3e as a function of corresponding group indexes in Fig. 3f, which shows good linearity confirming the linear dependence of light-dragging enhancement factor on the dispersion, i.e. group index as shown in Eq. (1).

Light drag enhanced by normal and anomalous dispersion. Both normal and anomalous dispersion enhanced light-dragging effect are demonstrated simultaneously in an SBS-induced

Fano-like transmission spectrum in Fig. 4. We realize such Fano-like transmission using the detuning technique^{19,28}, where the asymmetric Fano lineshape arises from the interference between two coupled resonances (optical one and acoustic one) and a coherent background^{28,33,34}. Such Fano resonance has a distinct asymmetric lineshape in the intensity spectrum (Fig. 4a) as well as the phase spectrum (Fig. 4b), which contains highly normal dispersive regimes on both wings but anomalous one in the center. As a result, the probe time delays are present on both wings, while turning to time advancement in the center (Fig. 4c). This opens up an opportunity to observe the light drag through these dispersion relations at the same time. The measured enhanced light drag now behaves oppositely to each other in terms of slope, with a ratio around -0.5 (Fig. 4d). In the meantime, the intracavity group index is estimated to be -1732 for the slow light regime and 3050 for the fast light regime calculated from the probe time delay/advancement in Fig. 4c. The ratio of group index in the two situations, calculated to be -0.57 , coincides with the slope ratio above. This is an important result since the dispersion-enhanced light drag can be easily flipped by a frequency detuning less than the linewidth of the resonance (acoustical one), opening up a new possibility for manipulating dispersion-enhanced light drag for sensing applications.

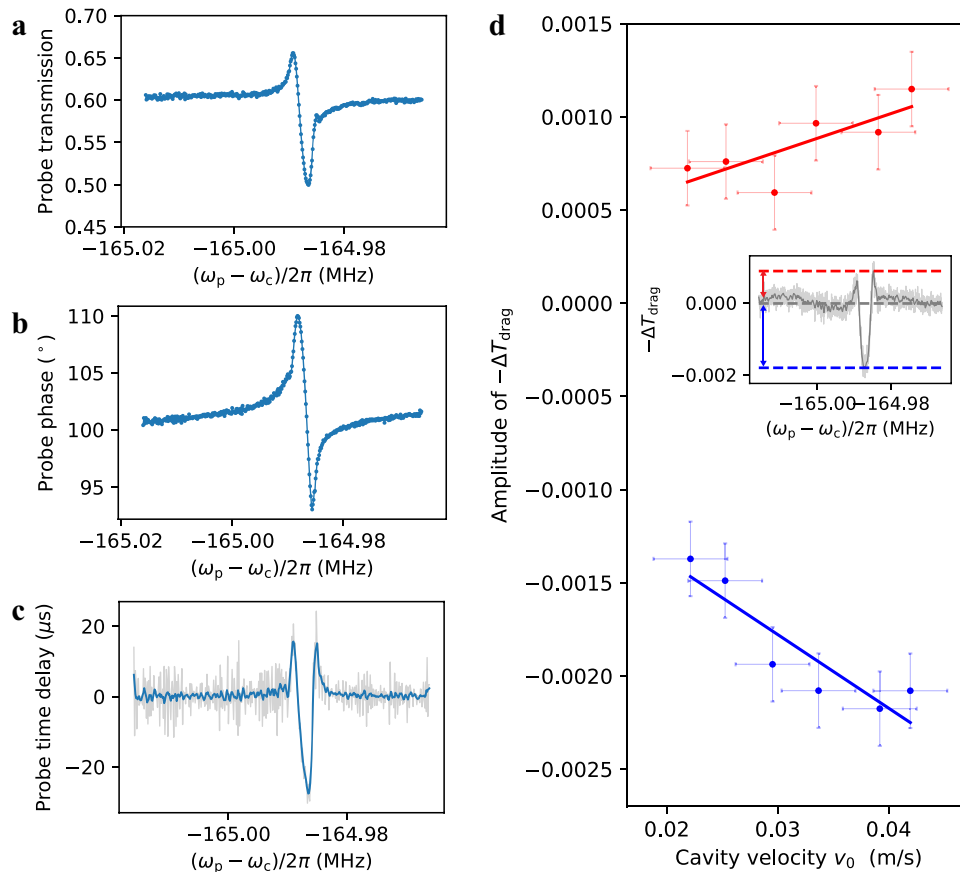


Fig. 4 Light-dragging effect with a Fano-like BSIA window. **a** A Fano-like transmission is observed with detuned control based on Brillouin scattering-induced absorption (BSIA). **b** The probe phase spectrum exhibits a negative slope at the center, while the positive slopes of wings are much steeper than the previous BSIA case. **c** The normal/anomalous dispersion gives rise to probe time delay/advancement. The maximum delay and advancement can be translated to intracavity group index of -1732 and 3050 , respectively. **d** Amplitude of the light-dragging-induced perturbation on probe transmission, ΔT_{drag} , is plotted as a function of cavity velocity with both slow-light and fast-light enhancement, where the enhancement of negative (red) and positive (blue) intracavity group index are showed by the slope of linear fits. The error bars represent the standard deviation of probe transmission (y-axis) and cavity velocity (x-axis).

Discussion

At last, we would like to discuss the potential applications of dispersion-enhanced light drag in motion sensing. Ideally, the current configuration can be directly applied for microscopic velocity sensing, i.e. velocimetry, which not only has a compact size comparable to devices based on micro-electro-mechanical systems but may also provide exceptional sensitivity (see Supplementary Note 1). Theoretically, combining with sensitive heterodyne detection and counter-propagating scheme, such dispersion-enhanced light-drag sensor can reach a sensitivity as low as $200 \text{ pm s}^{-1} \text{ Hz}^{-1/2}$, but with a limited travel range $\sim 1 \text{ mm}$ (constrained by coupling waveguide's length), which has already outperformed than many electrical/optical counterparts. On the other hand, if modifying the translational motion of the micro-cavity to a rotational one in the ref. ²⁵, we may also expect significant enhancement in rotation sensing. For the given configuration in this work, the corresponding rotational sensing ability can be theoretically estimated to be 9 degrees per hour with a millimeter-scale footprint (see Supplementary Note 1), which is sufficient for industrial metrology and motion-sensing applications. Moreover, a four-fold enhancement was reported recently in an exceptional-point-enhanced Sagnac gyro³⁵, which may also be considered for further improvement in sensitivity with dispersion enhancement³⁶. This implies a bright future of BSIT/BSIA enhanced rotation sensors due to its significant group index and controllability.

In summary, we have theoretically and experimentally examined Lorentz's prediction of dispersion-enhanced Fresnel light drag in both slow and fast light configurations. Compared with prior works, our new platform is implemented on a solid-state microcavity with a micrometer dimension (see Supplementary Note 9), thanks to a dispersion enhancement factor introduced by the BSIT/BSIA processes. Both fast-light-enhanced and slow-light-enhanced light drag has been demonstrated with a flexible tunability from active pumping or detuning, paving a way for compact applications in inertial, gyroscopic motional sensing.

Methods

Experimental system. The experimental system for this work is illustrated in Fig. 5. A taper-coupled microsphere optical cavity was used as a platform for studying dispersion-enhanced light drag. A control laser, generated by a continuously tunable laser with a center wavelength of 1550 nm , was used to pump up the forward Brillouin scattering. A probe laser, generated through an electro-optic modulator (EOM), was scanned near the SBS resonance to experience the dispersion and exhibit light drag. The network analyzer controlled the modulation frequency of EOM and monitors the amplitude, phase, and group time delay of the transmitted probe collected by a high-speed photodetector (PD), similar to prior works^{19,20}. The probe delay time recorded by the network analyzer was used to calculate the light-dragging enhancement factor F_d based on Supplementary Note 5.

A piezoelectric actuator was used to drive the microsphere cavity vibrating along the direction of the tapered fiber for the demonstration of light drag. The perturbation on probe transmission induced by the oscillating cavity was filtered and amplified by a lock-in amplifier. The piezo-driving signal and the reference signal for the lock-in amplifier were provided by two synchronized channels of a

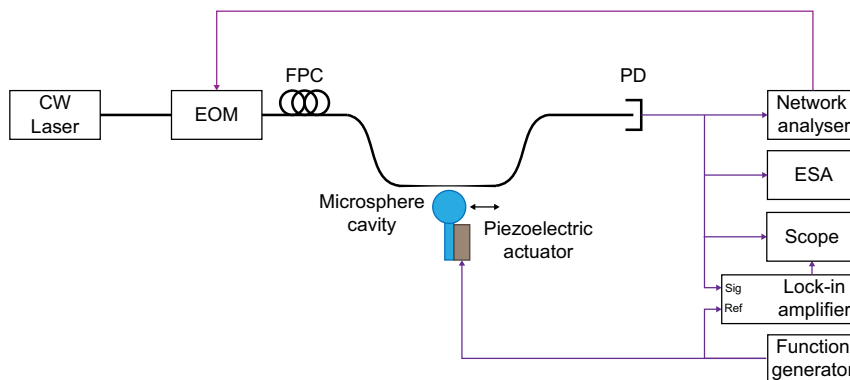


Fig. 5 The set-up for stimulated Brillouin scattering (SBS)-enhanced light-dragging experiment. A continuous-wave (CW) laser was used to generate the control signal. The probe signal was generated by a network analyzer through an electro-optic modulator (EOM). The control and the probe lasers were coupled in and out of the microsphere cavity via a tapered fiber. The optical transmission signal was received by a high-speed photodetector (PD) at the through port and the excitation of SBS was monitored on an electric spectrum analyzer (ESA). When SBS was excited, the amplitude, phase, and group time delay of the probe signal near the Brillouin resonance were measured by the network analyzer. A piezoelectric actuator was used to drive the microsphere cavity vibrating along the direction of the tapered fiber for the demonstration of light drag. The function generator generated the piezo-driving voltage and the reference signal for the lock-in amplifier. The lock-in amplifier was used to measure the amplitude of the perturbation on probe transmission led by light drag. FPC is the fiber polarization controller.

function generator. The perturbation on probe transmission consisted of a light-dragging part and a coupling-gap-modulation part, as mentioned in Supplementary Note 6. To get the light-dragging part, the probe frequency was scanned near BS resonance with a high repetition rate (4 Hz) for varying dispersion meanwhile the piezo-driving frequency was scanned slowly near the microcavity cantilever modes (at 10 mHz repetition rate) for varying vibration velocity. As the dispersion experienced by the probe was changed periodically by the fast scan of the probe laser, the dispersion enhanced light-dragging perturbation on probe transmission could be distinguished from the slowly varying background which did not respond to the change in dispersion.

Data availability

The data generated for the current study are available from the corresponding author upon reasonable request.

Received: 24 February 2020; Accepted: 3 June 2020;

Published online: 29 June 2020

References

- Einstein, A. On the electrodynamics of moving bodies. *Ann. Phys.* **17**, 50 (1905).
- Fresnel, A. J. Sur l'influence du mouvement terrestre dans quelques phenomenes d'optique: lettre de M. Fresnel a M. Arago. *Ann. Chim. Phys.* **9**, 57–66 (1818).
- Fizeau, H. Sur les hypotheses relatives à l'éther lumineux, et sur une expérience qui paraît démontrer que le mouvement des corps change la vitesse avec laquelle la lumière se propage dans leur intérieur. *C. R. Acad. Sci.* **33**, 349–355 (1851).
- Lorentz, H. A. Electromagnetic phenomena in a system moving with any velocity smaller than that of light. *Proc. K. Ned. Akad. Wet.* **6**, 809–831 (1904).
- Zeeman, P. Fresnel's coefficient for light of different colours (First part). *Proc. K. Ned. Akad. Wet.* **17**, 445–451 (1914).
- Zeeman, P. Fresnel's coefficient for light of different colours (Second part). *Proc. K. Ned. Akad. Wet.* **18**, 398–409 (1915).
- Norton, J. D. Einstein's investigations of Galilean covariant electrodynamics prior to 1905. *Arch. Hist. Exact Sci.* **59**, 45–105 (2004).
- Shahriar, M. S. et al. Ultrahigh enhancement in absolute and relative rotation sensing using fast and slow light. *Phys. Rev. A* **75**, 53807 (2007).
- Strekalov, D., Matsko, A. B., Yu, N. & Maleki, L. Observation of light dragging in a rubidium vapor cell. *Phys. Rev. Lett.* **93**, 23601 (2004).
- Safari, A., De Leon, I., Mirhosseini, M., Magaña-Loaiza, O. S. & Boyd, R. W. Light-drag enhancement by a highly dispersive rubidium vapor. *Phys. Rev. Lett.* **116**, 1–5 (2016).
- Kuan, P.-C., Huang, C., Chan, W. S., Kosen, S. & Lan, S.-Y. Large Fizeau's light-dragging effect in a moving electromagnetically induced transparent medium. *Nat. Commun.* **7**, 13030 (2016).
- Franke-Arnold, S., Gibson, G., Boyd, R. W. & Padgett, M. J. Rotary photon drag enhanced by a slow-light medium. *Science* **333**, 65–67 (2011).
- Carusotto, I., Artoni, M., La Rocca, G. C. & Bassani, F. Transverse Fresnel-Fizeau drag effects in strongly dispersive media. *Phys. Rev. A* **68**, 11 (2003).
- Soljačić, M. et al. Photonic-crystal slow-light enhancement of nonlinear phase sensitivity. *JOSA B* **19**, 2052–2059 (2002).
- Vlasov, Y. A., O'boyle, M., Hamann, H. F. & McNab, S. J. Active control of slow light on a chip with photonic crystal waveguides. *Nature* **438**, 65 (2005).
- Bahl, G., Zehnpfennig, J., Tomes, M. & Carmon, T. Stimulated optomechanical excitation of surface acoustic waves in a microdevice. *Nat. Commun.* **2**, 403 (2011).
- Weis, S. et al. Optomechanically induced transparency. *Science* **330**, 1520–1523 (2010).
- Safavi-Naeini, A. H. et al. Electromagnetically induced transparency and slow light with optomechanics. *Nature* **472**, 69 (2011).
- Dong, C.-H. et al. Brillouin-scattering-induced transparency and non-reciprocal light storage. *Nat. Commun.* **6**, 6193 (2015).
- Kim, J., Kuzyk, M. C., Han, K., Wang, H. & Bahl, G. Non-reciprocal Brillouin scattering induced transparency. *Nat. Phys.* **11**, 275–280 (2015).
- Turukhin, A. V. et al. Observation of ultraslow and stored light pulses in a solid. *Phys. Rev. Lett.* **88**, 23602 (2001).
- Bigelow, M. S., Lepeshkin, N. N. & Boyd, R. W. Superluminal and slow light propagation in a room-temperature solid. *Science* **301**, 200–202 (2003).
- Boyd, R. W. Slow and fast light: fundamentals and applications. *J. Mod. Opt.* **56**, 1908–1915 (2009).
- Terrel, M., Digonnet, M. J. F. & Fan, S. Performance comparison of slow-light coupled-resonator optical gyroscopes. *Laser Photon. Rev.* **3**, 452–465 (2009).
- Maayani, S. et al. Flying couplers above spinning resonators generate irreversible refraction. *Nature* **558**, 569–572 (2018).
- Knight, J. C., Cheung, G., Jacques, F. & Birks, T. A. Phase-matched excitation of whispering-gallery-mode resonances by a fiber taper. *Opt. Lett.* **22**, 1129 (1997).
- Xu, Q. et al. Experimental realization of an on-chip all-optical analogue to electromagnetically induced transparency. *Phys. Rev. Lett.* **96**, 123901 (2006).
- Zheng, Y. et al. Optically induced transparency in a micro-cavity. *Light Sci. Appl.* **5**, e16072 (2016).
- Fleischhauer, M., Imamoglu, A. & Marangos, J. P. Electromagnetically induced transparency: optics in coherent media. *Rev. Mod. Phys.* **77**, 633 (2005).
- Carmon, T., Yang, L. & Vahala, K. J. Dynamical thermal behavior and thermal self-stability of microcavities. *Opt. Express* **12**, 4742 (2004).
- Gorodetsky, M. L. & Ilchenko, V. S. Optical microsphere resonators: optimal coupling to high-Q whispering-gallery modes. *JOSA B* **16**, 147–154 (1999).
- Li, Y. L., Millen, J. & Barker, P. F. Simultaneous cooling of coupled mechanical oscillators using whispering gallery mode resonances. *Opt. Express* **24**, 1392–1401 (2016).
- Boller, K. J., Imamolu, A. & Harris, S. E. Observation of electromagnetically induced transparency. *Phys. Rev. Lett.* **66**, 2593–2596 (1991).
- Lezama, A., Barreiro, S. & Akulshin, A. M. Electromagnetically induced absorption. *Phys. Rev. A* **59**, 4732 (1999).
- Lai, Y.-H., Lu, Y.-K., Suh, M.-G., Yuan, Z. & Vahala, K. Observation of the exceptional-point-enhanced Sagnac effect. *Nature* **576**, 65 (2019).
- Scheuer, J. White light cavity formation and superluminal lasing near exceptional points. *Opt. Express* **26**, 32091 (2018).

Acknowledgements

This work was supported by National key research and development program (Grant Nos. 2016YFA0302500 and 2017YFA0303700); National Science Foundation of China (Grant Nos. 11674228 and 11304201). Shanghai MEC Scientific Innovation Program (Grant No. E00075); Shanghai Scientific Innovation Program (Grant No. 14JC1402900); Shanghai Scientific Innovation Program for International Collaboration (Grant No. 15220721400).

Author contributions

W.W. and T.Q. designed the study and wrote the manuscript. T.Q. assembled the experimental system, operated the experiment, and carried out initial analysis of data. J.Y., F.Z. helped with fabrication. Y.C., D.S., W.L., and L.C. assisted in designing the experimental system. X.J. and X.C. assisted with the theoretical model of the experiment. W.W. secured funding, analyzed results, and provided supervisory guidance. All authors reviewed the manuscript.

Competing interests

The authors declare no competing interests.

Additional information

Supplementary information is available for this paper at <https://doi.org/10.1038/s42005-020-0386-3>.

Correspondence and requests for materials should be addressed to W.W.

Reprints and permission information is available at <http://www.nature.com/reprints>

Publisher's note Springer Nature remains neutral with regard to jurisdictional claims in published maps and institutional affiliations.



Open Access This article is licensed under a Creative Commons Attribution 4.0 International License, which permits use, sharing, adaptation, distribution and reproduction in any medium or format, as long as you give appropriate credit to the original author(s) and the source, provide a link to the Creative Commons license, and indicate if changes were made. The images or other third party material in this article are included in the article's Creative Commons license, unless indicated otherwise in a credit line to the material. If material is not included in the article's Creative Commons license and your intended use is not permitted by statutory regulation or exceeds the permitted use, you will need to obtain permission directly from the copyright holder. To view a copy of this license, visit <http://creativecommons.org/licenses/by/4.0/>.

© The Author(s) 2020